Cell Research (2016) 26:674-685.

www.nature.com/cr

ORIGINAL ARTICLE

Signature motif-guided identification of receptors for peptide hormones essential for root meristem growth

Wen Song[1, *], Li Liu[2, *], Jizong Wang[1], Zhen Wu[1], Heqiao Zhang[1], Jiao Tang[1], Guangzhong Lin[1], Yichuan Wang[2, 3], Xing Wen[2], Wenyang Li[2], Zhifu Han[1], Hongwei Guo[2, 3], Jijie Chai[1]

[1]Innovation Center for Structural Biology, Tsinghua-Peking Joint Center for Life Sciences, School of Life Sciences, Tsinghua University, Beijing 100084, China; [2]The State Key Laboratory of Protein and Plant Gene Research, Peking-Tsinghua Joint Center for Life Sciences, Academy for Advanced Interdisciplinary Studies, College of Life Sciences, Peking University, Beijing 100871, China; [3]Department of Biology, South University of Science and Technology of China, Shenzhen, Guangdong 518055, China

Peptide-mediated cell-to-cell signaling has crucial roles in coordination and definition of cellular functions in plants. Peptide-receptor matching is important for understanding the mechanisms underlying peptide-mediated signaling. Here we report the structure-guided identification of root meristem growth factor (RGF) receptors important for plant development. An assay based on a signature ligand recognition motif (Arg-x-Arg) conserved in a subfamily of leucine-rich repeat receptor kinases (LRR-RKs) identified the functionally uncharacterized LRR-RK At4g26540 as a receptor of RGF1 (RGFR1). We further solved the crystal structure of RGF1 in complex with the LRR domain of RGFR1 at a resolution of 2.6 Å, which reveals that the Arg-x-Gly-Gly (RxGG) motif is responsible for specific recognition of the sulfate group of RGF1 by RGFR1. Based on the RxGG motif, we identified additional four RGFRs. Participation of the five RGFRs in RGF-induced signaling is supported by biochemical and genetic data. We also offer evidence showing that SERKs function as co-receptors for RGFs. Taken together, our study identifies RGF receptors and co-receptors that can link RGF signals with their downstream components and provides a proof of principle for structure-based matching of LRR-RKs with their peptide ligands.

Keywords: peptide hormone; RAM; RGF receptor; crystal structure; RxR motif

Cell Research (2016) **26**:674-685. doi:10.1038/cr.2016.62; published online 27 May 2016

Introduction

Small signaling peptides (~1 000) encoded in the *Arabidopsis thaliana* genome play essential roles in various aspects of plant growth and development [1-3]. By coordinating and integrating cellular functions, small plant peptides are important for cell-cell communication [2, 3]. The membrane-localized receptor kinases (RKs), the largest family of receptor-like molecules in plants [3], have been identified as specific receptors of various peptides, further underlining the importance of the small signaling peptides in plants. The largest subfamily of RKs contains an extracellular leucine-rich repeat (LRR) domain [4]. Signaling mediated by LRR-RKs, in many cases, requires somatic embryogenesis receptor-like kinases (SERKs) as co-receptors [5].

Root apical meristem, a region of the root tip consisting of undifferentiated cells, gives rise to different types of root cells, thus playing vital roles in regulating root pattern formation and adaptation to environmental stimuli [6, 7]. A family of 9-member small peptides called root meristem growth factors (RGFs) [8] or GOLVENs [9] or CLE-Ls [10] (hereafter called RGFs for simplicity) are important for the maintenance of root stem cell niche. RGFs are secreted peptides and matured through proteolytic processing of their precursor proteins and tyrosylprotein sulfotransferase (TPST)-catalyzed posttranslational tyrosine sulfation, which are required for the biological activity of RGFs [8]. RGF signaling-regulated expression and distribution of the transcription factors

*These two authors contributed equally to this work.
Correspondence: Jijie Chai[a], Hongwei Guo[b], Zhifu Han[c]
[a]E-mail: chaijj@tsinghua.edu.cn
[b]E-mail: hongweig@pku.edu.cn
[c]E-mail: hanzhifu@mail.tsinghua.edu.cn
Received 29 March 2016; revised 11 April 2016; accepted 20 April 2016; published online 27 May 2016

PLETHORAs (PLTs) are important for stem cell niche maintenance and root pattern formation [8, 11-13]. RGFs also play critical roles in regulating plant gravitropism [9, 14], lateral root and root hair formation [10, 15, 16], and sensitivity to phosphate deprivation [17].

Despite the important roles of RGFs in plant development, their receptors remain unidentified probably due to redundancy of the receptors, which renders genetic screening difficult. Here we applied an *in vitro* biochemical assay to identify the receptors of RGFs. Based on a signature small peptide recognition motif (RxR) conserved in a subfamily of LRR-RKs, we screened a pool of small peptides for their abilities to interact with the extracellular LRR domains of LRR-RKs from this subfamily. By this assay, we identified the functionally uncharacterized LRR-RK At4g26540 as a receptor of RGF1 (RGFR1), which was supported by a combination of biochemical, structural and genetic evidence. Additional four RGFRs were further identified based on a second structural motif, RxGG, responsible for specific recognition of the sulfate group of RGF1 as revealed by the crystal structure of the RGF1-RGFR1 complex. Identification of the receptors of RGFs will facilitate further dissection of RGF-induced signaling pathways. Furthermore, the screening strategy described here can be used to match RGF-like peptide ligands with their receptors in *Arabidopsis* and other plant species.

Results

Rationale for matching LRR-RLKs with their ligands

Many mature plant peptides including Peps from *Arabidopsis* (AtPeps) [18] have histidine or asparagine as the last residue [2]. Our previous study indicated that the last residue of AtPep1 is crucial for the recognition of this peptide by its receptor PEPR1, a member of the LRR XI subfamily [19]. This residue forms salt bridges with two arginines in the LRR-RK (RxR, x stands for any amino acid; hereafter called the RxR motif; Figure 1A). Intriguingly, the RxR motif is largely conserved in this subfamily of LRR-RKs (Figure 1B). Furthermore, several members of this LRR-RK subfamily have been shown to recognize small peptides ending with histidine or asparagine [20-25]. These findings prompted us to hypothesize that members of the LRR XI subfamily may act as receptors of small peptides with a free C-terminal histidine or asparagine. To identify ligands for LRR-RKs from this subfamily, we purified some extracellular LRR domains of these LRR-RKs and mixed each of them with a pool of chemically synthesized peptides featuring a free C-terminal histidine or asparagine (Supplementary information, Table S1). The mixture was then subjected to gel filtration (Supplementary information, Figure S1A). If a peptide interacts with an LRR protein, they are expected to co-migrate in gel filtration and the peptide will be separated from the others. The identity of the peptide was then determined by mass spectrometry (MS; Figure 1C). The previously reported HSL2-IDA [21] and PXY-TDIF [24] pairs were successfully matched (Supplementary information, Figure S1B) using this method, validating the reliability of the screening.

The LRR-RK At4g26540 functions as a receptor of RGFs in vitro

By using the method described above, we found that one of the peptides tested, RGF1, was co-purified with the extracellular LRR domain of the functionally uncharacterized LRR-RK At4g26540 (Supplementary information, Figure S1C), suggesting that this LRR-RK (hereafter called RGFR1) may function as a RGFR1. To further support this conclusion *in vitro*, we quantified the interaction between RGF1 and $RGFR1^{LRR}$ using microscale thermophoresis (MST). MST revealed a high binding affinity between RGF1 and $RGFR1^{LRR}$ with a dissociation constant (*K*d) of ~285 nM (Figure 1D). The interaction was further confirmed by the isothermal titration calorimetry (ITC) assay (Supplementary information, Figure S2A). When a non-sulfated RGF1 (dRGF1) was used for the MST assay, the interaction was significantly compromised (Figure 1D), supporting an important role of sulfation in RGF1 recognition by RGFR1. This is consistent with previous studies [8-10] showing that sulfation is required for the *in vivo* activity of RGF1 (Supplementary information, Figure S2B). In addition to RGF1, other eight RGFs also displayed interaction with $RGFR1^{LRR}$, but the $RGFR1^{LRR}$ binding affinities of RGFs 6, 7 and 9 were much lower than those of the other RGFs (Supplementary information, Figure S2C). To further confirm the RGF1-RGFR1 interaction, we solved the crystal structure of RGF1 in complex with $RGFR1^{LRR}$ at a resolution of 2.6 Å (Figures 1E, 2A and Supplementary information, Table S2). Structural comparison reveals that RGF1 and AtPep1 interact with their respective receptors in a conserved manner (Figure 1E). As hypothesized, the RxR motif of RGFR1 interacts with the free carboxyl group of the last residue $RGF1^{Asn13}$ (Figure 1E). Similar to the interaction between AtPep1 and its receptor, the RxR motif of RGFR1 is also important for RGFR1 recognition of RGF1, as the double mutation R458A/R460A of the RxR motif nearly abolished the RGF1-binding activity of $RGFR1^{LRR}$ as indicated by MST (Figure 1D).

Recognition mechanism of RGFs by RGFRs

In the structure, RGF1 adopts a fully extended confor-

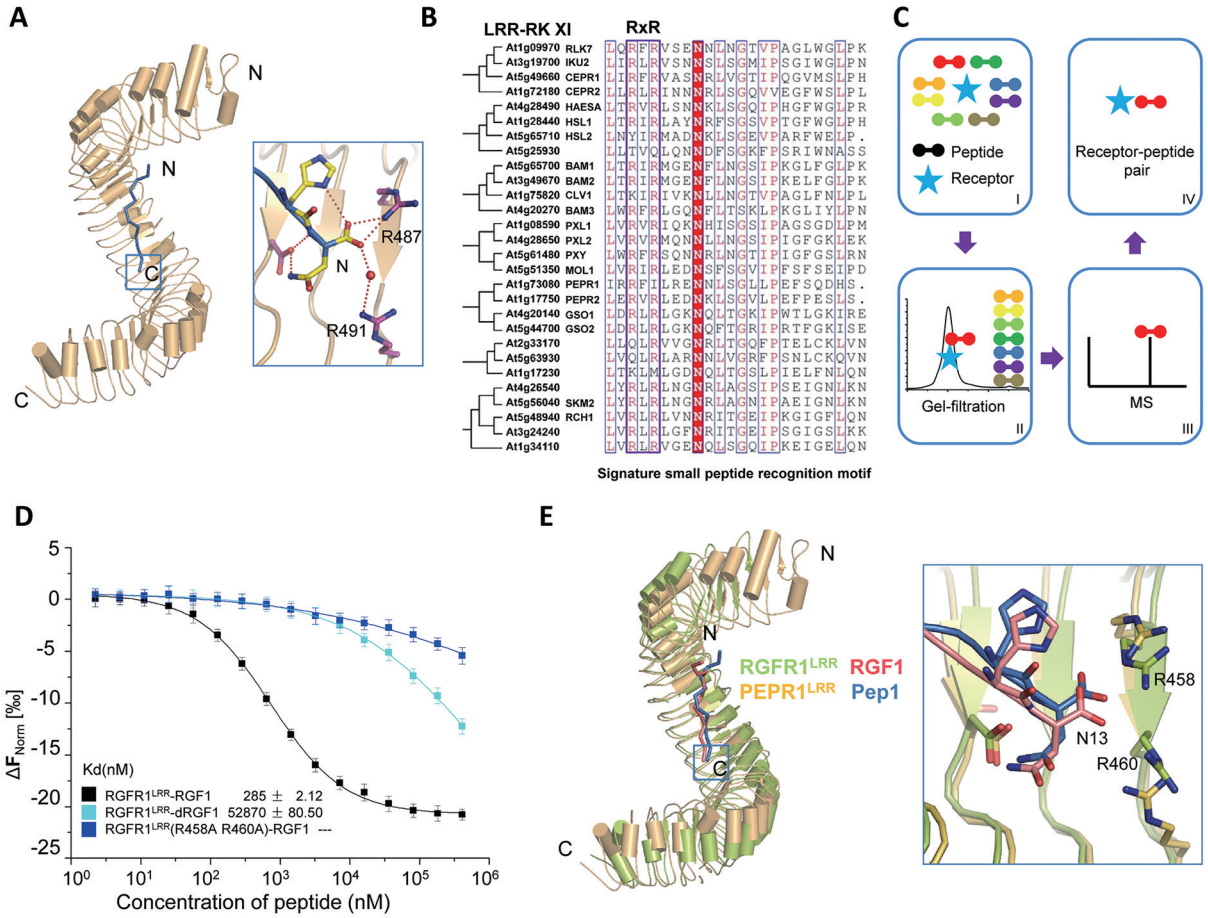

Figure 1 RxR motif-based identification of the LRR-RK At4g26540 as a receptor of RGF1 *in vitro*. **(A)** The RxR motif is used by the LRR-RK AtPEPR1 to recognize AtPep1. Left, overall structure of AtPep1-PEPR1^{LRR} complex. Right, detailed interactions of the boxed region in the left panel. The side chains of the last residue from AtPep1 and the RxR motif from PEPR1 are labeled. Color codes are indicated. **(B)** Sequence alignment of LRRs harboring the RxR motif among the LRR XI subfamily of LRR-RKs in *Arabidopsis*. **(C)** A schematic diagram showing RxR motif-based identification of the peptide-receptor pair. A purified extracellular LRR domain of an XI LRR-RK is incubated with a pool of peptides (box I) and then subjected to gel filtration (box II). The peak fraction is collected for MS (box III). The peptide identified by MS is regarded as the potential ligand for the LRR-RK (box IV). **(D)** RGF1 interacts with the LRR domain of the LRR-RK At4g26540 (RGFR1) *in vitro*. Quantification of the binding affinity between RGF1 and RGFR1^{LRR} by MST. Data points indicate the differences in normalized fluorescence (%) generated by RGF1 binding to RGFR1^{LRR}, and curves indicate the calculated fits. Error bars represent standard error of 3 independent measurements. dRGF1: non-sulfated RGF1. **(E)** RGFR1 and AtPEPR1 share a conserved ligand recognition mode. Left, structural superposition of the RGF1-RGFR1^{LRR} and AtPep1-AtPEPR1^{LRR} complexes. Right, detailed interactions of the last residues of RGF1 and AtPep1 with their respective receptors. The side chains of the last residue of RGF1 and the RxR motif of RGFR1 are labeled.

mation and its charge closely matches the electrostatic surface potential of RGFR1^{LRR} (Figure 2A and 2B). The conserved N- and C-terminal portions of RGF1 interact with two positive patches of the peptide-binding groove of RGFR1^{LRR}, whereas the less conserved central region of RGF1 binds a negatively charged surface of the groove (Figure 2B). In addition to the RxR motif, RGFR1^{Asp412} and RGFR1^{Leu436} are also involved in recognition of the last residue RGF1^{Asn13} by forming hydrogen bonds and Van der waals contact with this peptide residue, respectively (Figure 2C). Interaction of RGF1^{Asn13} with RGFR1^{LRR} is further strengthened by RGFR1^{Trp390} that packs against the side chain of RGF1^{Asn13}. The sulfate group of RGF1^{Tyr2} binds to a positively charged pocket of RGFR1 (Figure 2D), further supporting our biochemical data (Figure 1D). RGFR1^{Arg195} appears important for recognition of the sulfate group because three salt bridges are formed between them. In addition, the sulfate

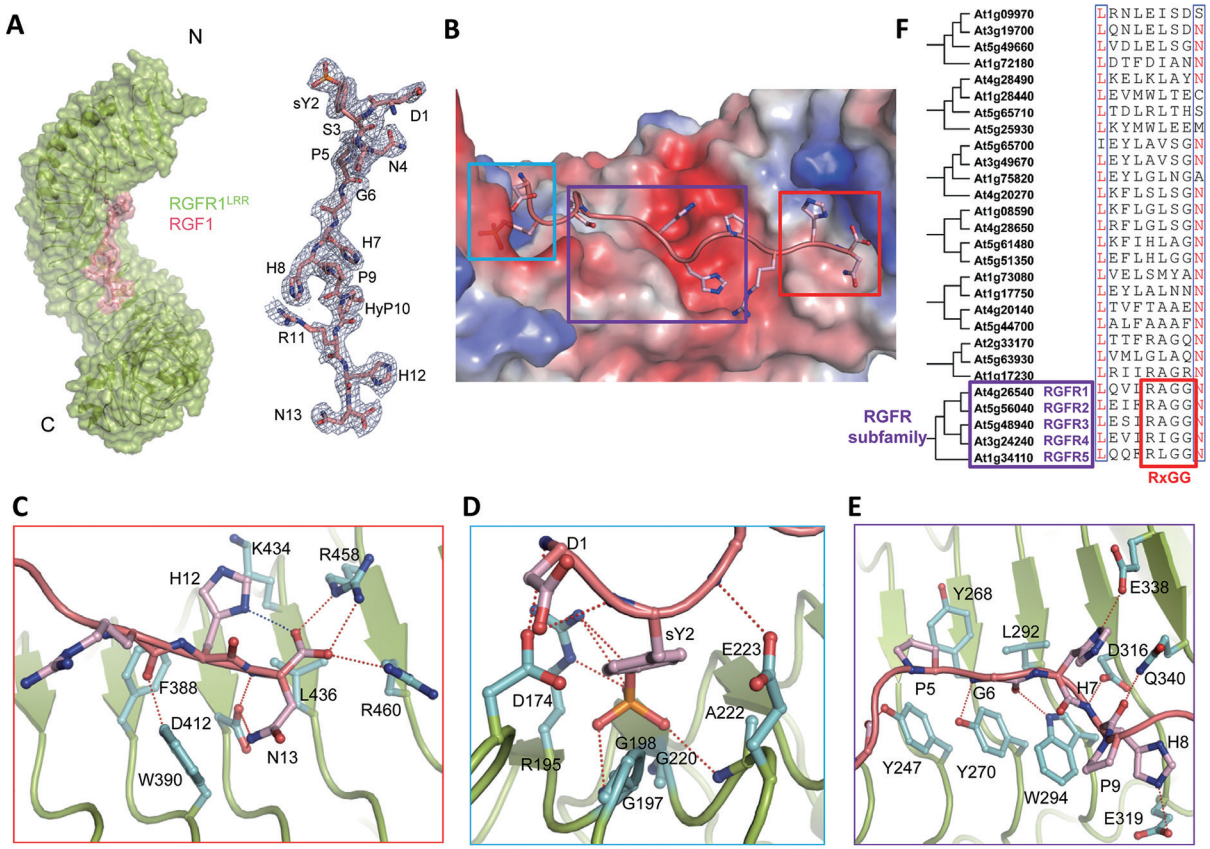

Figure 2 Recognition mechanism of RGF1 by RGFR1. **(A)** Left, overall structure of the RGF1-RGFR1^{LRR} complex shown in cartoon. RGFR1^{LRR} and RGF1 are shown in lemon and pink, respectively. Right, finally refined electron density "*2Fo-Fc*" contoured at 1.20 σ surrounding RGF1. HyP: hydroxylated proline; sY: sulfated tyrosine. **(B)** RGF1 binds to a charged surface groove at the inner side of the RGFR1^{LRR} solenoid. RGFR^{LRR} is shown in electrostatic surface and RGF1 is shown in cartoon. Red, blue and white indicate negative, positive and neutral surfaces, respectively. **(C)** Recognition of the last residue of RGF1 by RGFR1^{LRR}. Red dashed lines indicate hydrogen bonds or salt bridges. **(D)** Recognition of the sulfated RGF1^{Tyr2} by RGFR1. The side chains of RGFR1^{LRR} and RGF1 are shown in green and pink, respectively. **(E)** Recognition of the central part of RGF1 by RGFR1^{LRR}. The side chains of RGFR1^{LRR} and RGF1 are shown in cyan and pink, respectively. **(F)** Sequence alignment of the LRRs (the sixth LRR) containing the RxGG motif among the XI subfamily of LRR-RKs in *Arabidopsis*. The RxGG motif is highlighted within the red square. Five genes containing the RxGG motif were identified as receptors of RGFs and named RGFRs 1-5, and the subfamily of these five genes was named RGFR subfamily.

group also establishes polar interactions with the amide nitrogen atoms of RGFR1^{Gly197} and RGFR1^{Ala222}. The Van der waals contacts formed between the sulfate group and RGFR1^{Gly220} further fortify the RGF1^{Tyr2}-RGFR1 interactions. RGFR1^{Gly198} packs tightly against the benzene ring of RGF1^{Tyr2} from the underneath (Figure 2D). Therefore, RGFR1^{Gly198} and RGFR1^{Gly197} appear to have an important role in specific recognition of the sulfated RGF1 through steric effect. In addition, RGFR1^{Asp174} forms a hydrogen bond and a salt bridge with the amide nitrogen of RGF1^{Tyr2} and the free amine of RGF1^{Asp1}, respectively (Figure 2D). In comparison with RGF1^{Tyr2}, the side chain of RGF1^{Asp1} is completely solvent-exposed, consistent with the observation that RGF4 with isoleucine at this position (different from the other 8 RGFs which all start with Asp) still displayed interaction with RGFR1 (Supplementary information, Figure S2C). A combination of hydrogen bonding and hydrophobic packing mediates RGFR1 recognition of the central part of RGF1 (Figure 2E). Crystal structures of RGFR1 in complex with other three RGF peptides (RGFs 2, 3 and 5) further confirm the conserved recognition mechanism of RGFs by RGFR1 (Supplementary information, Figure S3).

Structure-based sequence alignment reveals that the residues (RGFR1^{Arg195}, RGFR1^{Gly197} and RGFR1^{Gly198}, hereafter called the RxGG motif) responsible for specific recognition of the sulfate group of RGF1 are unique to these five LRR-RKs including RGFR1 (Figure 2F),

which belong to the same cluster in the LRR XI subfamily (Figure 1B). Furthermore, all the other RGF1-interacting residues are also highly conserved among these five LRR-RKs (Supplementary information, Figure S4). These results suggest that, in addition to RGFR1, the other four LRR-RKs (named RGFR2, at5g56040; RGFR3, at5g48940; RGFR4, at3g24240; RGFR5, at1g34110) may also recognize RGFs. Although we were unable to express the extracellular LRR domains of three of these LRR-RKs (RGFRs 3-5), the purified LRR domain of RGFR2 (called SKM2 in a previous study [26]) interacted with RGF1 in both gel filtration and MST assays (Supplementary information, Figure S5).

RGF receptors control root meristem development

To provide evidence for the conclusion that RGFRs 1-5 function as receptors of RGFs in plants, we generated five RGFR Promoter::GUS lines. Expression pattern analysis revealed that all the five RGFRs were expressed in roots (Figure 3). Transcription of RGFR1 was mainly restricted to columella, transition zone and root stem cell niche, whereas expression of RGFR2 was detected in the transition, elongation and differentiation zones of the roots (Figure 3 and Supplementary information, Figure S6). By contrast, whole roots were found to highly express RGFRs 3-5 (Figure 3). In addition, expression of RGFR2 was also detected in flowers and stipules, and RGFR5 expression was detected in hypocotyl (Supplementary information, Figure S7). Thus, the expression patterns of RGFRs are similar to those of RGFs in plants (Supplementary information, Figure S7) [15], consistent with their possible interaction *in vivo*.

To analyze the functions of RGFRs in root meristem development, we generated seven homozygous mutant lines of *Arabidopsis*, the single mutants *rgfr1* (Salk_053167), *rgfr2* (Salk_057829), *rgfr3* (Salk_038309), *rgfr4* (Salk_040393), and *rgfr5* (Salk_014726) (Supplementary information, Figure S8), and the double mutants *rgfr1 rgfr2* and *rgfr3 rgfr4*. Phenocopying the *rgf1 rgf2 rgf3* triple mutants [8], the *rgfr1, rgfr2, rgfr3, rgfr4* and *rgfr5* single mutant seedlings had smaller meristem sizes and fewer meristematic cortex cells compared with wild-type plants (Figure 4A), but a more severe meristem defect was found in the *rgfr5* mutant plants (Figure 4A). The *rgfr1 rgfr2* and *rgfr3 rgfr4* double mutant plants exhibited more severe phenotypes than each of their single mutants (Figure 4A), suggesting redundant roles of these receptors in maintaining the meristem size of *Arabidopsis*. These results were also consistent with their overlapping but not identical expression patterns (Figure 3). The mutant plants also exhibited short root phenotypes (Figure 4B). Differences in meristematic cortex cell number and root length among the single mutant plants suggest that RGFRs may have varied roles in regulating meristem and root growth (Figure 4A and 4B). As observed before [8, 10, 16], wild-type plants responded to RGF1 in a dose-dependent biphasic manner, with low doses stimulating growth and high doses inhibiting growth (Supplementary information, Figure S9). Treatment with 1.0 nM of RGF1 almost restored the meristematic cortex cell numbers of the single mutants *rgfr1*, *rgfr2* and *rgfr3* to the levels of wild-type plants (Supplementary information, Figure S10), but root length appeared slightly less sensitive to RGF1 in these mutants (Figure 4C). By contrast, the same concentration of dRGF1 did not have a stimulating effect on the numbers of meristematic cortex cells in *rgfr1* and *rgfr2* mutant plants (Figure 4D). These results indicate that the root meristem defects in the RGFR mutant plants are RGF-specific. Notably, the double mutants *rgfr1 rgfr2*

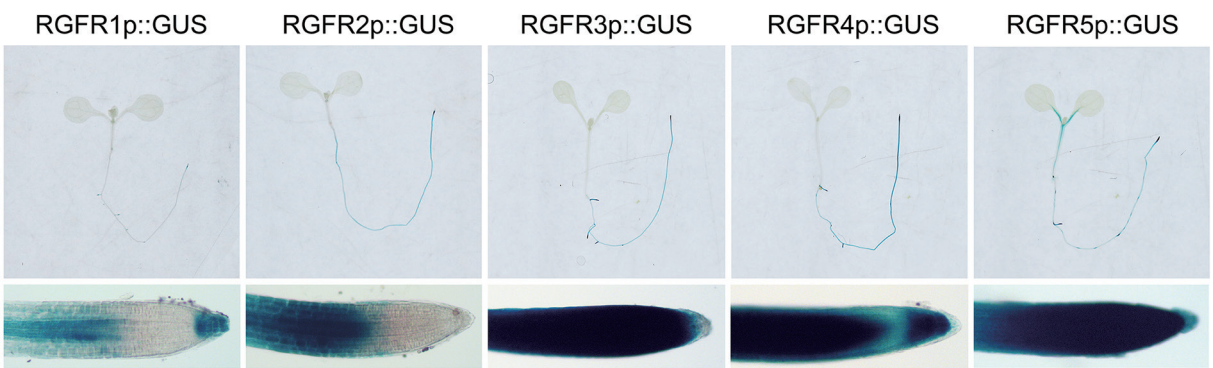

Figure 3 Expression patterns of RGFRs in root. The expression patterns of RGFR1p::GUS, RGFR2p::GUS, RGFR3p::GUS, RGFR4p::GUS and RGFR5p::GUS, in green seedlings (top) and root tips (bottom).

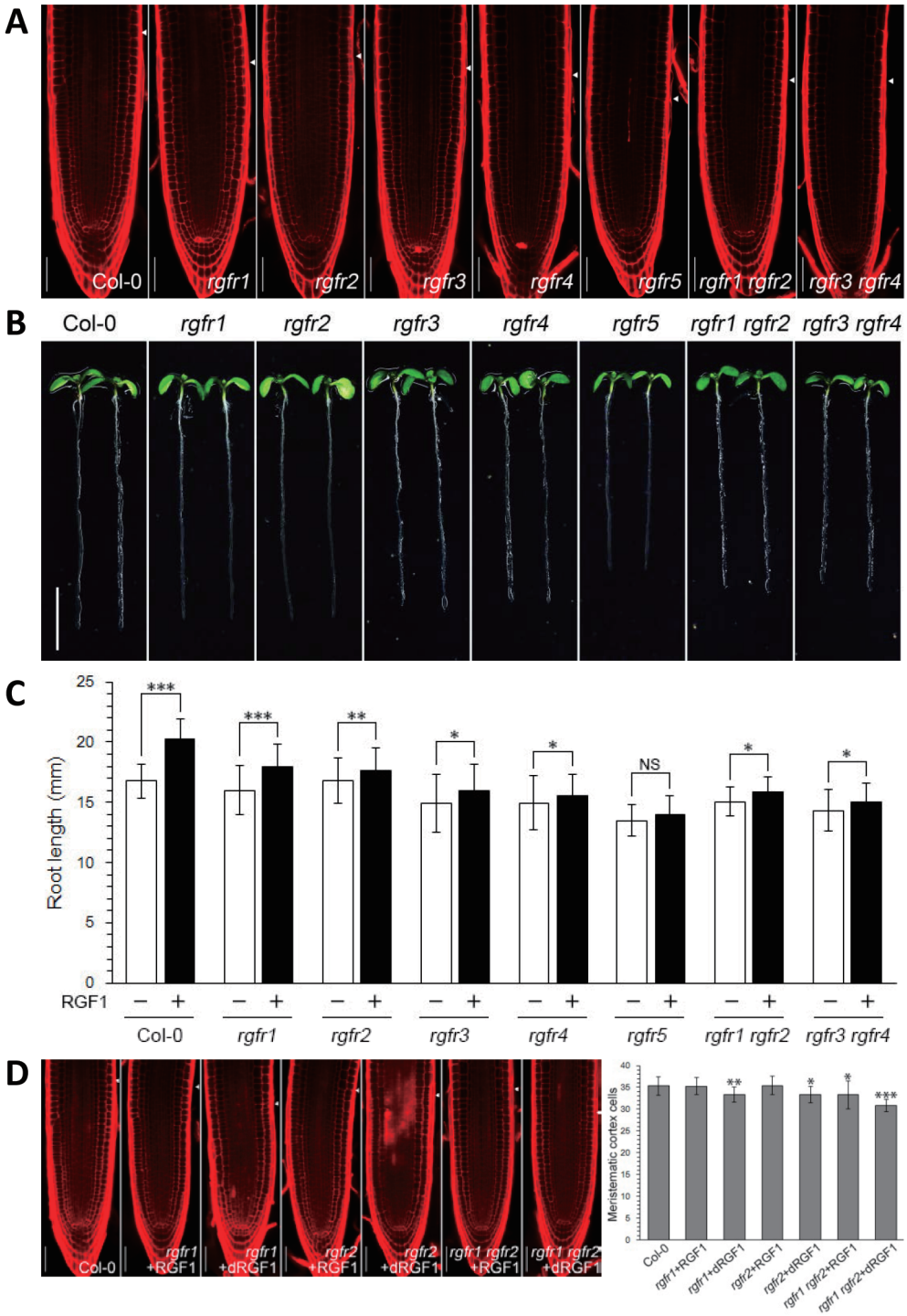

Figure 4 Loss-of-function *rgfr* mutants exhibit defects in root meristem and deceased sensitivity to RGF1. **(A)** Confocal images of the root meristem of Col-0 and mutants (5 DAG stage). The white arrowhead indicates the boundary of meristematic zone and elongation zone. Scale bar, 50 μm. **(B)** Root lengths of Col-0 and mutant seedlings (7 DAG stage). **(C)** Changes of root lengths of Col-0 and *rgfr* mutants in response to RGF1. Quantification of root lengths of Col-0 and mutant seedlings (7 DAG stage) grown in the medium supplied with 1 nM RGF1. **(D)** Quantification of root meristem cells of Col-0 and mutant seedlings (5 DAG stage) grown in the medium supplied with 1 nM RGF1 or dRGF1. $n = 25$. *$P < 0.05$, **$P < 0.01$, ***$P < 0.001$ by Student's *t*-test. NS indicates not significant.

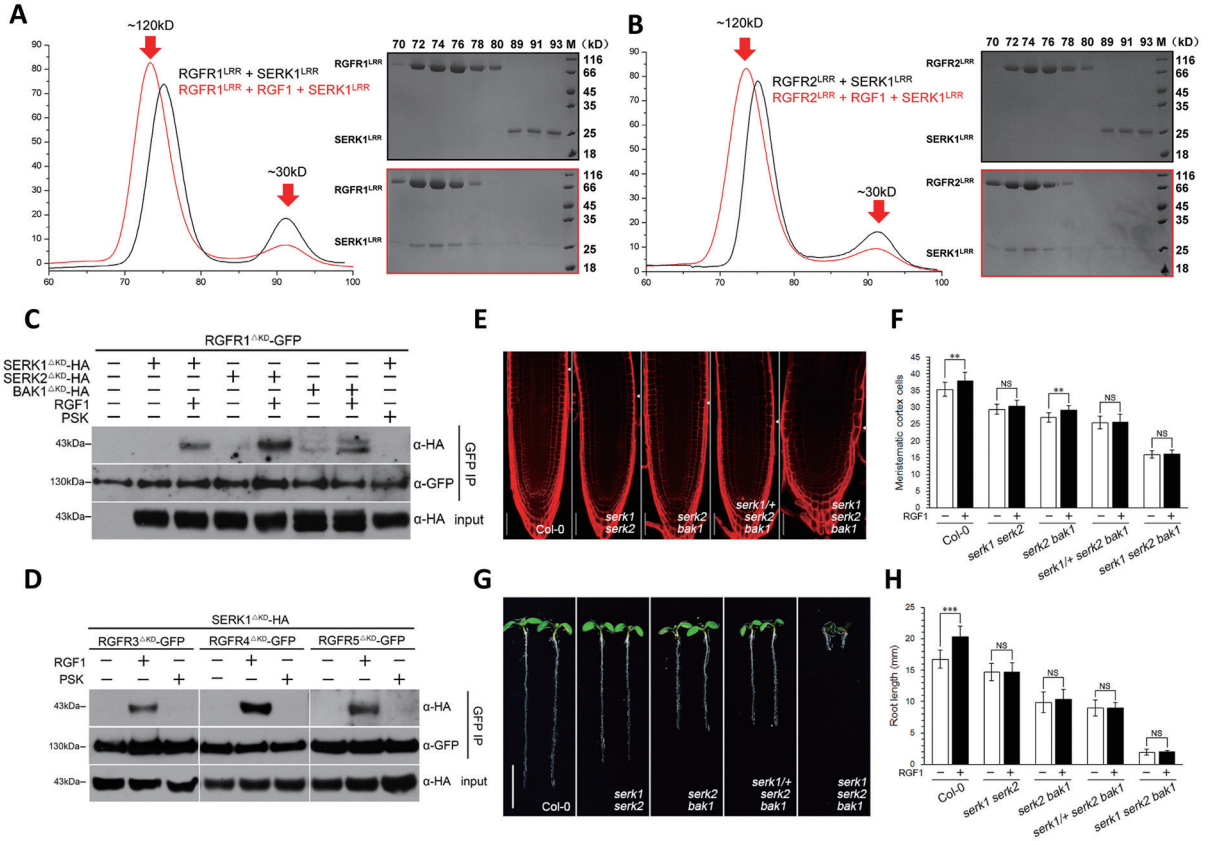

Figure 5 Identification of SERKs as co-receptors for RGF1. **(A)** RGF1 induces RGFR1^{LRR}-SERK1^{LRR} interaction *in vitro*. Left, superposition of the gel filtration chromatograms of the RGFR1^{LRR}+SERK1^{LRR} and RGFR1^{LRR}+RGF1+SERK1^{LRR} proteins. The vertical and horizontal axes represent UV absorbance (280 nm) and elution volume (ml), respectively. Right, coomassie blue staining of the peak fractions shown on the left following SDS-PAGE. M, molecular weight ladder (kDa). **(B)** RGF1 induces RGFR2^{LRR}-SERK1^{LRR} interaction *in vitro*. Left, superposition of the gel filtration chromatograms of the RGFR2^{LRR}+SERK1^{LRR} and RGFR2^{LRR}+RGF1+SERK1^{LRR} proteins. **(C)** RGF1 promotes RGFR1$^{\Delta KD}$-SERK1$^{\Delta KD}$/SERK2$^{\Delta KD}$/BAK1$^{\Delta KD}$ interaction in *Nicotiana Benthamiana*. Agrobacteria harboring the indicated constructs were syringe infiltrated into tobacco leaves. Peptides (10 nM RGF1, 1 μM PSK as a negative control) were added 2 h before tobacco tissues were harvested for immunoprecipitation with anti-GFP antibody. Immunoblot assays were performed to determine the levels of expressed proteins. Each assay was repeated three times. **(D)** RGF1 promotes RGFR3$^{\Delta KD}$-SERK1$^{\Delta KD}$, RGFR4$^{\Delta KD}$-SERK1^{KD} and RGFR5$^{\Delta KD}$-SERK1$^{\Delta KD}$ interaction in *Nicotiana Benthamiana*. **(E)** Confocal images of the root meristem of Col-0 and mutants (5 DAG stage). The white arrowheads indicate the boundary of meristematic zone and elongation zone. Scale bar, 50 μm. **(F)** Changes in meristematic cortex cell numbers in Col-0 and *serk* mutants in response to RGF1. Quantification of meristematic cortex cell number of Col-0 and mutant seedlings (5 DAG stage) grown in the medium supplied with 1 nM RGF1. n = 25. **(G)** Root lengths of Col-0 and *serk* mutant seedlings (7 DAG stage). **(H)** Changes in root lengths of Col-0 and *serk* mutants in response to RGF1. Quantification of root lengths of Col-0 and mutant seedlings (7 DAG stage) grown in the medium supplied with 1 nM RGF1. n = 25. *P < 0.05, **P < 0.01, ***P < 0.001 by Student's t-test. NS indicates not significant.

and *rgfr3 rgfr4* were much less sensitive to the same concentration of RGF1 than single mutant plants in meristem growth (Figure 4C and Supplementary information, Figure S10), further supporting a redundant role of these four RGFRs in regulating meristem development. Interestingly, the single mutant *rgfr5* was also less sensitive to the same concentration of RGF1 than the other four single mutants (Figure 4C and Supplementary information, Figure S10), suggesting that it might play a more important role in meristem development.

SERK family members as co-receptors with RGFs

RGF1 binding induced no RGFR1 homodimerization (Supplementary information, Figure S11), suggesting that a co-receptor is required for RGF1-induced signaling based on the dimerization model [5]. The C-termini of

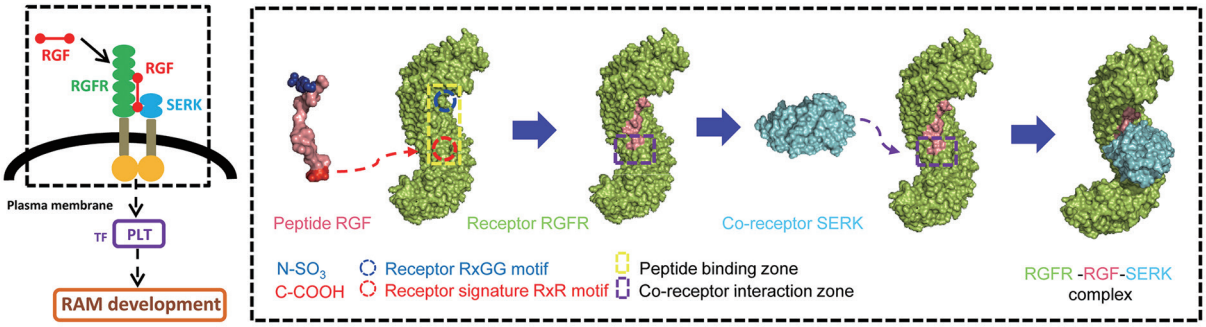

Figure 6 Model of RGF signaling initiation. Cartoon illustration showing RGF-induced RGFR activation. The N- (blue) and C-terminal (red) sides of an RGF interact with the RGF-specific motif RxGG and the peptide-determining motif RxR of an RGFR, respectively. The surface formed by the conserved RxR motif of the RGFR and the last residue of the RGF could recruit a SERK member as a co-receptor.

AtPep1 and TDIF mediate interaction of a SERK member with AtPEPR1 [19] and PXY [27], respectively. Given the conserved C-termini of AtPep1, TDIF and RGF1, and the conserved RxR motif of AtPEPR1 and RGFRs, RGFRs might also use SERK members as co-receptors. This hypothesis is consistent with the observation that SERK members play critical but brassinosteroid-independent roles in root meristem activities [28]. Gel-filtration results showed that RGF1 induced the interaction between RGFR1^{LRR} or RGFR2^{LRR} and SERK1/2/BAK1^{LRR} (Figure 5A, 5B and Supplementary information, Figure S12), further strengthening our conclusion that RGFRs 1 and 2 function as receptors of RGF1. In contrast, dRGF1 or the RGFR1^{LRR} mutant proteins with much lower RGF1-binding activity failed to do so under the same conditions (Supplementary information, Figure S12). Besides RGF1, several other RGFs but not RGFs 6, 7 and 9 also induced RGFR1^{LRR} interaction with SERK1^{LRR} (Supplementary information, Figure S13). RGF1-induced RGFR1-SERK interaction was also detected in *Nicotiana Benthamiana* expressing the kinase domain (KD)-truncated RGFR1$^{\Delta KD}$-GFP and SERK1/SERK2/BAK1$^{\Delta KD}$-HA (Figure 5C). Similarly, RGFR3$^{\Delta KD}$, RGFR4$^{\Delta KD}$ and RGFR5$^{\Delta KD}$ also interacted with SERK1$^{\Delta KD}$ in the presence of RGF1 stimulation (Figure 5D), which further confirmed that these three LRR-RKs act as receptors of RGFs.

To investigate whether SERKs are important for RGF-induced signaling in plants, we generated four mutant plants, *serk1 serk2*, *serk2 bak1*, *serk1/+ serk2 bak1* and *serk1 serk2 bak1*. In consistence with our biochemical data, all these mutants exhibited smaller meristems and shorter roots (Figure 5E and 5G) than wild-type plants, which were also observed in the *rgfr* (Figure 4A and 4B) and *rgf1,2,3* [8] mutants. More importantly, these *serk* mutants except for *serk2 bak1* almost lost their responsiveness to RGF1 (Figure 5F and 5H), indicating that SERKs are important for RGF1-induced signaling. This result also suggests that *serk1* may have a more important role in meristem growth. Together with our biochemical results, these genetic data show that SERKs act as co-receptors for RGFRs in RGF-induced signaling to regulate root meristem development.

Discussion

Matching ligand-receptor pair is crucial to understand LRR-RK-mediated signaling pathways. Unfortunately, only a small number of ligand-receptor pairs have been characterized thus far and progress in this respect via genetic approaches has been hampered by the redundancy of both receptors and ligands. Here we set up a signature motif-based biochemical assay to match a subfamily of LRR-RKs with their ligands. By this assay, we identified RGFRs 1-5 from this LRR-RK subfamily as receptors of RGFs. This conclusion is supported by a combination of biochemical, structural and genetic evidence. While the assay remains to be further optimized, finding of the signature small peptide recognition motif RxR conserved in a subfamily of LRR-RKs would facilitate the identification of their ligands in *Arabidopsis*. Given that this structural motif is highly conserved across plant species (Supplementary information, Figure S14), a similar assay is in principle applicable to match LRR-RKs with their ligands in species other than *Arabidopsis*.

Our data suggest a model of RGF-induced RGFR activation (Figure 6). In addition to interaction with the RxR motif of an RGFR, the C-terminus of an RGF may also be involved in recruitment of a SERK member as a co-receptor. The conserved RxGG motif is important for RGFRs to distinguish RGFs from other similar peptides.

It is conceivable that other members of the LRR XI subfamily of LRR-RKs may also possess unique motifs, in addition to the conserved RxR motif, to specifically recognize their ligands. In contrast to the N- and C-terminal ends, the central region of RGFs is much less conserved. Several RGFs were shown to bind RGFR1 but with different affinities. These results suggest that the non-conserved region of RGFs is an affinity-determining epitope for their receptors. It would be interesting to investigate whether other subfamilies of LRR-RKs or even other types of RKs have similar sequences to the RxR and RxGG motifs in RGFRs, which can be utilized for ligand recognition. We wish to mention that the *in vitro* interaction of RGF1 with RGFRs is much weaker compared with the potency of RGF1 in plant-based assays. The precise reason for this discrepancy is unclear; however, this type of discrepancy is common in studies of single transmembrane receptors such as PSKR [29]. One possible explanation is that the plant-based assays contained all the RGF signaling components including their full-length receptors and co-receptors, whereas our *in vitro* binding assays (MST and ITC) used the purified protein of the extracellular domain of RGFR1. Probably the intracellular environment is favorable for RGF interaction with its receptors.

Five receptors (RGFRs 1-5) are involved in RGF signaling and their overlapping but not identical expression patterns (Figure 3 and Supplementary information, Figure S7) suggest that they may have both redundant and distinct roles in regulation of plant development. This is reminiscent of CLE signaling that has multiple peptide signals and receptors to control cell proliferation and differentiation [3]. Although future studies on further matching of RGFs with RGFRs in plants are needed, our data suggest the diversity of the RGF signaling, which likely involves specific recognition of different sets of RGFs by different RGFRs, thus regulating distinct downstream targets (e.g., PLT and PIN) in plant development. Despite different receptor preferences, many of the nine RGFs strongly interacted with RGFR1 *in vitro*, but their distinct expression patterns may dictate selective activation of specific receptors. Future studies aiming to identify other components in the RGF signaling are expected to reveal how the RGF signaling specificity is achieved *in vivo*.

During the preparation of the manuscript, three LRR-RLKs, corresponding to RGFRs 1, 3 and 4 identified in the current study, were reported to be involved in RGF perception [30]. In addition, an accompanying study [31] identified the same five LRR-RLKs as receptors for RGFs by using a completely different approach from ours, further supporting the validity of our biochemical assay for matching of receptors and their ligands. In conclusion, our study not only identifies RGF receptors and reveals SERKs as co-receptors with RGFRs, but also opens the possibility of matching other XI LRR-RK members with their ligands using the conserved R-x-R motif.

Materials and Methods

Protein expression and purification

Sequences encoding the LRR domains of the RKs RGFR1, RGFR2, PXY, HSL2, GSO1, SERK1, SERK2 and BAK1 from *Arabidopsis* with C-terminal 6× His tag were generated by standard PCR-based cloning strategy and their identities were confirmed by sequencing. All the LRR proteins were expressed in High Five cells at 22 °C using the vector pFastBac (Invitrogen). One liter of cells (2×10^6 cells/ml cultured in the medium from Expression Systems) was infected with 30 ml baculovirus of a specific protein and the media was harvested after 60 h of infection. All the proteins were first purified using Ni-NTA (Novagen). The bound proteins were eluted and further purified by size-exclusion chromatography (Hiload 200, GE Healthcare) in buffer containing 10 mM Bis-Tris pH 6.0, 100 mM NaCl.

Peptide synthesis

The peptides (Supplementary information, Tables S1) were chemically synthesized by the Scilight-Peptide Company (Beijing, China). Peptides were dissolved in double distilled water to a final stock concentration of 20.0 mg/ml for biochemical and genetic assays.

Gel filtration and MS assays

Approximately 0.5 mg of purified different LRR domain proteins (in 1.0 ml buffer containing 10 mM Bis-Tris pH 6.0, 100 mM NaCl) were individually incubated with a peptide mixture (0.1 mg for each; Supplementary information, Table S1) on ice for 1 h. Then each of the mixtures was analyzed by gel filtration (Superdex 200, GE Healthcare), the peak fraction was collected and 2 µl was used for MALDI TOF-MS. To test RGF-induced interaction between the $RGFR1^{LRR}$ (wild type or mutants) and the $SERK1^{LRR}$, the two purified proteins as described above were mixed with a molar ratio of ~1:2 ($RGFR1^{LRR}$:$SERK1^{LRR}$) in buffer containing 10 mM Bis-Tris pH 6.0, 100 mM NaCl. The mixture was incubated on ice for 1 h and then subjected to gel filtration analysis (Hiload 200, GE Healthcare) in the presence (molar ratio of $RGFR1^{LRR}$:$SERK1^{LRR}$:RGF ~1:2:5) or absence of an RGF. Samples from relevant fractions were applied to SDS-PAGE and visualized by Coomassie blue staining. Similar protocols were used to assay RGF-induced $RGFR1/2^{LRR}$ interaction with $SERK2^{LRR}$ or $BAK1^{LRR}$.

Crystallization, data collection and structure determination

To crystallize $RGFR1^{LRR}$ in complex with RGF1, the purified $RGFR1^{LRR}$ protein was concentrated to about 10.0 mg/ml and mixed with chemically synthesized RGF1 at a molar ratio of ~1:10, and the mixture was incubated on ice for 3 h. Crystals of the complex were generated by the hanging-drop vapor-diffusion method. The drops were set up with 1 µl $RGFR1^{LRR}$ plus 1 µl reservoir solution at 18 °C. Diffraction quality crystals of the $RGFR1^{LRR}$-RGF1 complex were obtained in buffer containing 0.1 M MES monohydrate pH 6.0, 22% (v/v) polyethylene glycol (PEG)

400. Similar conditions were used for crystallization of $RGFR1^{LRR}$ in complex with RGF2, RGF3 or RGF5. The diffraction data sets were collected at the Shanghai Synchrotron Radiation Facility (SSRF) on beam line BL17U1 using a CCD detector. All the data were processed using HKL2000 [32]. The crystal structure of $RGFR1^{LRR}$-RGF1 was determined by molecular replacement (MR) with PHASER [33] using the structure of $FLS2^{LRR}$ (PDB code: 4MN8) as the initial searching model. The model from MR was built with the program COOT [34] and subsequently subjected to refinement by the program Phenix [35]. All the remaining structures were solved by using the refined structure of the $RGFR1^{LRR}$-RGF1 as the initial model for MR and refined with Phenix. All the figures representing structures were prepared using PYMOL [36].

MST assay

The MST assay was used to measure the affinity of the purified $RGFR1^{LRR}$, $RGFR2^{LRR}$ or $RGFR1^{LRR}$ mutant proteins with RGFs by the Monolith NT.115 from Nanotemper Technologies [37]. All the proteins were fluorescently labeled according to the manufacturer's protocol and the labeled protein used for each assay was about 200 nM. A solution of unlabeled RGFs (Supplementary information, Table S1) was diluted to an appropriate serial concentration gradient. After incubation at room temperature for 30 min, a labeled protein and the diluted peptide were loaded into silica capillaries (Polymicro Technologies). Measurements were performed at 20 °C in buffer containing 10 mM citric acid pH 6.0, 100 mM NaCl, and 0.05% Tween 20, by using 12% LED power and 40% MST power. The assays were repeated three times for each affinity measurement. Data analyses were performed using Nanotemper Analysis software and OriginPro 8.0 software.

ITC

To further verify the interaction between the $RGFR1^{LRR}$ protein and RGF1, ITC200 was used to quantify their binding affinity. All of the samples for ITC were prepared in a buffer containing 10 mM HEPES, pH 6.0, 100 mM NaCl and titrations were executed at 25 °C. 0.1 mM $RGFR1^{LRR}$ was titrated against 1 mM RGF1. All the ITC data were analyzed using MicroCal Origin 7.0.

Plant materials

The ecotype Columbia (Col-0) was the parent strain for all mutants and transgenic lines used in this study. The *rgfr1*, *rgfr2, rgfr3*, *rgfr4* and *rgfr5* mutants were brought from ABRC (https://abrc.osu.edu/). The double mutants *rgfr1 rgfr2* and *rgfr3 rgfr4* were generated by genetic cross. The *serk1 serk2*, *serk2 bak1* and *serk1/+ serk2 bak1* mutants were generously provided by Dr Weicai Yang (Institute of Genetics and Developmental Biology, Chinese Academy of Sciences), and *serk1 serk2 bak1* mutant was generated by genetic cross. Transgenic seedlings were obtained through Agrobacterium-mediated transformation of *Arabidopsis thaliana* using the floral dip method [38] in wild-type Col-0. Transgenic plants were screened with 50 μg/ml kanamycin on Murashige and Skoog (MS) medium. Homozygous lines were identified by calculating offspring segregation ratio by GUS or fluorescence observation. At least three independent transgenic lines were used in each experiment.

Growth condition and drug treatment

Arabidopsis seeds were plated on MS medium after surface-sterilization in 70% ethanol and 0.1% Triton X-100. The plates were stored at 4 °C for 3 days, and then kept in an incubator with a 16/8 h light/dark cycle at 22 °C in 70% humidity to grow until the seedlings were transferred into soil.

For root length measurement and histochemistry analysis, seeds were plated on 1/2 MS medium in petri dishes with or without different concentration of RGFs. The dishes were vertically placed in incubator with usual conditions.

Root length measurement

For quantitative root length measurements, images of 7 DAG seedlings were captured using digital camera. Roots of more than 20 seedlings were measured using ImageJ software (NIH). Values shown are average lengths (means ± 2 SEM) of roots. Three independent experiments were performed.

Microscopy and histochemistry analysis

For confocal microscopic analysis, 5 DAG green seedlings were stained with 10 μM propidium iodide for 5 min, washed gently in double distilled water, and mounted on glass slides to visualize at 600-640 nm for propidium iodide or 500-560 nm for GFP under a confocal microscope (Zeiss LSM710). The numbers of root meristematic cells were obtained by counting the cortex cell from the cell proximal to the QC to rapid elongated cell.

For detailed tissue observation of GUS staining, tissues were mounted on glass slides and observed using Olympus CX31 optical microscope system.

Construction of plasmids

About 2-kb DNA sequence upstream of start codon (ATG) of RGFRs 1-5 were amplified by PCR as their respective promoter sequences. Primers are listed in (Supplementary information, Table S3). pBI101 vector was used to construct promoter::GUS plasmid.

Full-length coding region of RGFRs 1-5 were amplified from *Arabidopsis* cDNA, which was reverse transcribed from Col-0 RNA. GFP sequence was amplified from plasmid pEGAD-GFP, and then engineered at 3′-end of RGFR1/2 with a linker (GGAGGA). RGFR1-GFP fusion sequence was inserted into *Bam*HI and *Kpn*I sites, followed by insertion of RGFR1 promoter into *Hin*dIII and *Bam*HI sites. RGFR2-GFP fusion sequence was inserted into *Kpn*I and *Sal*I sites, followed by insertion of RGFR2 promoter into *Hin*dIII and *Kpn*I sites.

The KD-truncated SERK1, SERK2 and BAK1 were amplified from *Arabidopsis* cDNA. An HA tag (TATCCTTACGACGTGCCTGACTACGCC) was fused at the 3′-end of the sequence. The PCR product was inserted into *Sac*I and *Kpn*I sites of the binary vector pCAMBIA1307 (a derivative of pCAMBIA1300 by inserting CaMV 35S promoter sequence prior to multiple cloning site) to generate construct of pCAMBIA1307-SERK1/SERK2/BAK1ΔKD-HA.

GUS staining

About 2 kb promoter sequence of RGFR1-5 were amplified by PCR, and cloned into pBI101 vector to generate the constructs. The constructs were transformed into *Arabidopsis* wild-type Col-0 to generate stable transgenic lines. At least three independent transgenic lines of each gene were analyzed for GUS staining at 5 DAG, 8 DAG, 20 DAG and mature stage.

The seedlings or tissues were collected, washed with staining

buffer without X-Gluc, stained with GUS staining buffer (50 mM sodium phosphate buffer, pH 7.0, 10 mM Na_2EDTA, 0.5 mM $K_4[Fe(CN)_6]\cdot 3H_2O$, 0.5 mM $K_3[Fe(CN)_6]$, 0.1% Triton X-100, and 1 mg/ml X-Gluc), incubated at 37 °C for 2 h, and then ethanol (70%) was used to terminate the staining reaction. Some tissues were cleared in chloral hydrate solution (chloral hydrate:water:glycerol = 8:3:1; w/v/v) for 5 min for detailed observation.

Transient expression in Nicotiana benthamiana

Transient expression in *N. benthamiana* was performed as described previously [39]. Agrobacterium strains (GV3101) harboring above-described constructs were cultured in liquid Luria-Bertani medium overnight. The dense cultures were inoculated into fresh medium by 1:100 dilution and incubated for 6-8 h. The bacteria were pelleted and resuspended in infiltration buffer (5 g/L glucose, 10 mM $MgCl_2$, 10 mM MES-KOH, pH 5.7; adding 150 μM acetosyringone right before use) to an OD_{600} of 0.4. The resuspended agrobacteria was infiltrated into tobacco leaves using 1 ml syringes without needles. For coexpression, resuspended bacteria containing different constructs were mixed with equal OD_{600} of 0.4. After 46 h, 10 nM RGF1 or 1 μM PSK [30] was infiltrated into tobacco leaves, while double-distilled water was infiltrated as mock. All leaves were harvested after 2 h of infiltration.

Co-immunoprecipitation and immunoblot assays

The expression of proteins of interest was tested by immunoblot assays at first. The tobacco leaves were rapidly frozen in liquid nitrogen after harvest, and grinded into fine powder. A fraction of powder was added with an equal volume of 2× SDS sample buffer (4% SDS, 100 mM Bis-Tris pH 6.8, 10% glycerol, 2% β-mercaptoethanol), and incubated in ice for 15 min, following by boiling at 65 °C for 10 min. After centrifugation at 13 000× *g* for 5 min, the protein extracts were fractionated by 10% SDS-PAGE, blotted onto a PVDF membrane. Immunoblot assay was then performed using anti-GFP antibody (Beijing TDY) and anti-HA antibody (Santa Cruz).

For co-immunoprecipitation, 500 μl well-expressed sample was distributed in each tube and homogenized in 1.5 ml ice cold IP buffer (50 mM Bis-Tris pH 7.5, 150 mM NaCl, 1 mM DTT, 1 mM EDTA, 0.1% NP-40, 1× protease cocktail inhibitor (Sigma)) for 15 min. Lysates were centrifuged twice at 13 000× *g* at 4 °C for 10 min. For input sample, 80 μl supernatant was transferred to a new tube and 20 μl of 5× SDS sample buffer (10% SDS, 250 mM Bis-Tris pH 6.8, 50% glycerol, 5% β-mercaptoethanol, and 0.05% bromophenol blue) was added. In all, 1.2 ml supernatant was transferred to a new tube to incubate with 10 μl GFP-trap agarose beads (Chromo Tec, Cat# Gta-200) for 2 h in 4 °C under gentle agitation. Next, the beads were washed six times with IP buffer, and centrifuged at 2 000× *g* at 4 °C for 2 min each time. A total of 60 μl 5× SDS sample buffer was added after the last wash. Subsequently, all the samples were boiled at 65 °C for 10 min. Proteins were separated by SDS-PAGE and analyzed by immunoblot assays using anti-HA antibody and anti-GFP antibody. Images were captured by Kodak MXP-102 or Tanon 5200 Multi chemiluminescent imaging system (Tanon, Shanghai, China).

Accession codes

The atomic coordinates and structure factors have been deposited in the Protein Data Bank (PDB). The PDB codes of RGF1-RGFR1^{LRR}, RGF2-RGFR1^{LRR}, RGF3-RGFR1^{LRR} and RGF5-RGFR1^{LRR} are 5HYX, 5HZ0, 5HZ1 and 5HZ3, respectively.

Acknowledgments

We thank S Huang and J He at Shanghai Synchrotron Radiation Facility (SSRF) for assistance with data collection; H Deng and J Liu at the center for Biomedical Analysis of Tsinghua University for MS analysis; L Li and A Jiang at Peking University for providing the incubator. We acknowledge the Tsinghua University Branch of China National Center for Protein Sciences Beijing for providing the facility support. This work was funded by Projects of International Cooperation and Exchanges of the National Natural Science Foundation of China (31420103906), the Ministry of Science and Technology of China (2015CB910200) and State Key Program of the National Natural Science of China (31130063 and 31421001) to JC; the National Natural Science Foundation of China (91217305 and 91017010) to HG.

Author Contributions

JC, HG, ZH, WS and LL designed the experiments; WS and LL performed the experiments; ZH, JW, ZW, HZ, JT, GL, YW, XW and WL provided help for the experiments. JC, HG, ZH, WS and LL analyzed the data; JC, HG, ZH, WS and LL contributed to manuscript preparation; JC, WS and ZH wrote the manuscript.

Competing Financial Interests

The authors declare no competing financial interests.

References

1 Lease KA, Walker JC. The *Arabidopsis* unannotated secreted peptide database, a resource for plant peptidomics. *Plant Physiol* 2006; **142**:831-838.
2 Matsubayashi Y, Sakagami Y. Peptide hormones in plants. *Annu Rev Plant Biol* 2006; **57**:649-674.
3 Grienenberger E, Fletcher JC. Polypeptide signaling molecules in plant development. *Curr Opin Plant Biol* 2015; **23**:8-14.
4 Shiu SH, Bleecker AB. Plant receptor-like kinase gene family: diversity, function, and signaling. *Sci STKE* 2001; **2001**:22.
5 Han Z, Sun Y, Chai J. Structural insight into the activation of plant receptor kinases. *Curr Opin Plant Biol* 2014; **20**:55-63.
6 Petricka JJ, Winter CM, Benfey PN. Control of *Arabidopsis* root development. *Annu Rev Plant Biol* 2012; **63**:563-590.
7 Aichinger E, Kornet N, Friedrich T, Laux T. Plant stem cell niches. *Annu Rev Plant Biol* 2012; **63**:615-636.
8 Matsuzaki Y, Ogawa-Ohnishi M, Mori A, Matsubayashi Y. Secreted peptide signals required for maintenance of root stem cell niche in *Arabidopsis*. *Science* 2010; **329**, 1065-1067
9 Whitford R, Fernandez A, Tejos R, *et al.* GOLVEN secretory peptides regulate auxin carrier turnover during plant gravitropic responses. *Dev Cell* 2012; **22**:678-685.
10 Meng L, Buchanan BB, Feldman LJ, Luan S. CLE-like (CLEL) peptides control the pattern of root growth and lateral root development in *Arabidopsis*. *Proc Natl Acad Sci USA* 2012; **109**:1760-1765.
11 Aida M, Beis D, Heidstra R, *et al.* The PLETHORA genes mediate patterning of the *Arabidopsis* root stem cell niche.

Cell 2004; **119**, 109-120.
12 Galinha C, Hofhuis H, Luijten M, *et al.* PLETHORA proteins as dose-dependent master regulators of *Arabidopsis* root development. *Nature* 2007; **449**, 1053-1057.
13 Mahonen AP, Tusscher K, Siligato R, *et al.* PLETHORA gradient formation mechanism separates auxin responses. *Nature* 2014; **515**:125-129.
14 Gilroy S. Plant tropisms. *Curr Biol* 2008; **18**:R275-R277.
15 Fernandez A, Drozdzecki A, Hoogewijs K, *et al.* Transcriptional and functional classification of the GOLVEN/ROOT GROWTH FACTOR/CLE-like signaling peptides reveals their role in lateral root and hair formation. *Plant Physiol* 2013; **161**:954-970.
16 Fernandez A, Drozdzecki A, Hoogewijs K, *et al.* The GLV6/RGF8/CLEL2 peptide regulates early pericycle divisions during lateral root initiation. *J Exp Bot* 2015; **66**, 5245-5256.
17 Cederholm HM, Benfey PN. Distinct sensitivities to phosphate deprivation suggest that RGF peptides play disparate roles in *Arabidopsis thaliana* root development. *New Phytol* 2015; **207**:683-691.
18 Huffaker A, Pearce G, Ryan CA. An endogenous peptide signal in *Arabidopsis* activates components of the innate immune response. *Proc Natl Acad Sci USA* 2006; **103**:10098-10103.
19 Tang J, Han Z, Sun Y, Zhang H, Gong X, Chai J. Structural basis for recognition of an endogenous peptide by the plant receptor kinase PEPR1. *Cell Res* 2015; **25**:110-120.
20 Ogawa M, Shinohara H, Sakagami Y, Matsubayashi Y. *Arabidopsis* CLV3 peptide directly binds CLV1 ectodomain. *Science* 2008; **319**:294.
21 Stenvik GE, Tandstad NM, Guo Y, *et al.* The EPIP peptide of inflorescence deficient in abscission is sufficient to induce abscission in *Arabidopsis* through the receptor-like kinases HAESA and HAESA-LIKE2. *Plant Cell* 2008; **20**:1805-1817.
22 Tabata R, Sumida K, Yoshii T, Ohyama K, Shinohara H, Matsubayashi Y. Perception of root-derived peptides by shoot LRR-RKs mediates systemic N-demand signaling. *Science* 2014; **346**:343-346.
23 Yamaguchi Y, Pearce G, Ryan CA, *et al.* The cell surface leucine-rich repeat receptor for AtPep1, an endogenous peptide elicitor in *Arabidopsis*, is functional in transgenic tobacco cells. *Proc Natl Acad Sci USA* 2006; **103**:10104-10109.
24 Etchells JP, Turner SR. The PXY-CLE41 receptor ligand pair defines a multifunctional pathway that controls the rate and orientation of vascular cell division. *Development* 2010; **137**:767-774.
25 Hou S, Wang X, Chen D, *et al.* The secreted peptide PIP1 amplifies immunity through receptor-like kinase 7. *PLoS Pathog* 2014; **10**:e1004331.
26 Endo S, Shinohara H, Matsubayashi Y, Fukuda H. A novel pollen-pistil interaction conferring high-temperature tolerance during reproduction via CLE45 signaling. *Curr Biol* 2013; **23**:1670-1676.
27 Du J, Yin H, Zhang S, *et al.* Somatic embryogenesis receptor kinases control root development mainly via brassinosteroid-independent actions in *Arabidopsis thaliana*. *J Integr Plant Biol* 2012; **54**:388-399.
28 Zhang H, Lin X, Han Z, Qu L, Chai J. Crystal structural of PXY-TDIF complex reveals a conserved recognition mechanism among CLE peptide-receptor pairs. *Cell Res* 2016; **26**:543-55
29 Wang J, Li H, Han Z, *et al*. Allosteric receptor activation by the plant peptide hormone phytosulfokine. *Nature* 2015; **525**:265-268.
30 Shinohara H, Mori A, Yasue N, Sumida K, Matsubayashi Y, Identification of three LRR-RKs involved in perception of root meristem growth factor in *Arabidopsis*. *Proc Natl Acad Sci USA* 2016; **113**:3897-3902.
31 Ou Y, Lu X, Zi Q, *et al*. RGF1 INSENSITIVE 1 to 5, a group of LRR receptor-like kinases, are essential for the perception of root meristem growth factor 1 in *Arabidopsis thaliana*. *Cell Res*. 2016 May 27. doi: 10.1038/cr.2016.63
32 Otwinowski Z, Minor W. Processing of X-ray diffraction data collected in oscillation mode. *Methods Enzymol* 1997; **276**:307-326.
33 McCoy AJ, Grosse-Kunstleve RW, Adams PD, Winn MD, Storoni LC, Read RJ. Phaser crystallographic software. *J Appl Crystallogr* 2007; **40**:658-674.
34 Emsley P, Cowtan K. Coot: Model-building tools for molecular graphics. *Acta Crystallogr D Biol Crystallogr* 2004; **60**:2126-2132.
35 Adams PD. PHENIX: Building new software for automated crystallographic structure determination. *Acta Crystallogr D Biol Crystallogr* 2002; **58**:1948-1954.
36 DeLano WL. PyMOL Molecular Viewe 2002 (http://www.pymol.org).
37 Jerabek-Willemsen M, Wienken CJ, Braun D, Baaske P, Duhr S. Molecular interaction studies using microscale thermophoresis. *Assay Drug Dev Technol* 2011; **9**:342-353.
38 Clough SJ, Bent AF. Floral dip: a simplified method for Agrobacterium-mediated transformation of *Arabidopsis thaliana*. *Plant J* 1998; **16**:735-743.
39 Sparkes IA, Runions J, Kearns A, Hawes C. Rapid transient expression of fluorescent fusion proteins in tobacco plants and generation of stably transformed plants. *Nat Protoc* 2006; **1**:2019-2025.

(**Supplementary information** is linked to the online version of the paper on the *Cell Research* website.)